Anomalous orbital magnetism in Dirac-electron systems: Role of pseudospin paramagnetism

Mikito Koshino and Tsuneya Ando
Department of Physics, Tokyo Institute of Technology, 2-12-1 Ookayama, Meguro-ku, Tokyo 152-8551, Japan
(Received 23 February 2010; revised manuscript received 16 April 2010; published 25 May 2010)

The orbital diamagnetic susceptibility is calculated in monolayer and bilayer graphenes with band gap as well as in three-dimensional Dirac systems. It is demonstrated that the pseudospin degree of freedom such as valleys produces paramagnetic susceptibility analogous to contribution from real spin, and it dominates over the Landau diamagnetism. The pseudospin paramagnetism explains the origin of a singular diamagnetism which is present only in the band-gap region and disappears rapidly inside the conduction and valence bands.

DOI: 10.1103/PhysRevB.81.195431 PACS number(s): 81.05.ue, 75.20.−g, 75.70.Ak

I. INTRODUCTION

The magnetism of conventional metal is composed of two different contributions: the spin component known as the Pauli paramagnetism and the orbital component known as the Landau diamagnetism. In condensed-matter systems, the orbital magnetism sensitively depends on the detail of the electronic band structure, and sometimes largely deviates from the Landau diamagnetism. Particularly, narrow gap materials such as graphite[1–3] or bismuth[4–6] exhibit a singular behavior in the orbital susceptibility near the energy gap. In this paper, we show that the anomalous orbital magnetism in narrow gap systems can be understood in terms of pseudospin paramagnetism, which arises from the extra degree of freedom in the orbital motion of electrons.

Graphene monolayer recently fabricated[7–9] is a zero-gap system in which the conduction and valance bands stick together at K and K' points located at inequivalent corners of the Brillouin zone, called valleys.[1,10–17] The system is characterized by chiral quasiparticles with opposite chirality in each valley and a linear dispersion reminiscent of massless Dirac fermions. At the Dirac point where two bands cross each other, the magnetic susceptibility has a singularity expressed as a δ function in Fermi energy ε_F.[1,18–24] Bilayer graphene composed of a pair of graphene layers[25–28] has a zero-gap structure with a finite mass,[29–37] leading to a less singular logarithmic peak of the susceptibility.[38,39] The orbital magnetism was also studied for related materials, such as graphite intercalation compounds,[38,40–42] carbon nanotube,[43–46] few-layer graphenes,[39,47,48] and organic compounds having Dirac-like spectrum.[49]

In this paper, we calculate the orbital magnetism of several Dirac-like systems with an energy gap and show that the pseudospin degree of freedom such as valleys in graphene produces paramagnetism, which gives an essential contribution to the singular diamagnetic behavior. In Sec. II, we calculate the susceptibility of the monolayer graphene with varying gap. The singular susceptibility change in varying ε_F is understood in terms of valley-induced paramagnetism. We extend the analysis to the bilayer graphene in Sec. III and to a three-dimensional Dirac system corresponding to bismuth[4–6,50] in Sec. IV. A brief conclusion is presented in Sec. V.

II. MONOLAYER GRAPHENE

Graphene is composed of a honeycomb network of carbon atoms, where a unit cell contains a pair of sublattices, denoted by A and B. Electronic states in the vicinity of K and K' points in the Brillouin zone are well described by the effective-mass approximation.[1,10–17] Let $|A\rangle$ and $|B\rangle$ be the Bloch functions at the K point, corresponding to the A and B sublattices, respectively. In a basis $(|A\rangle,|B\rangle)$, the Hamiltonian for the monolayer graphene around the K point becomes[1,10–17]

$$\mathcal{H}^K = \begin{pmatrix} \Delta & v\pi_- \\ v\pi_+ & -\Delta \end{pmatrix}, \tag{1}$$

where $v \approx 1\times 10^6$ m/s is the band velocity,[8,9] $\pi_\pm = \pi_x \pm i\pi_y$, and $\boldsymbol{\pi} = -i\hbar\boldsymbol{\nabla} + (e/c)\mathbf{A}$ with vector potential $\mathbf{A}$ giving external magnetic field $\mathbf{B} = \boldsymbol{\nabla}\times\mathbf{A}$. In the following, we shall completely neglect the spin Zeeman energy because the spin splitting is much smaller than Landau-level separations. The Hamiltonian at the K' point is obtained by exchanging $\pi_\pm$ in Eq. (1).

The diagonal terms $\pm\Delta$ represent the potential asymmetry between A and B sites, which opens an energy gap at the Dirac point.[12,51] This can arise in graphene placed on a certain substrate material, where the interaction between the graphene and the substrate lattice produces different potentials between A and B. In fact, a band gap on the order of 0.1 eV has been observed in graphene epitaxially grown on a SiC substrate.[52,53] From a theoretical point of view, the singular behavior in ideal graphene with vanishing gap is better understood by taking the limit $\Delta \to 0$, as will be shown below. We can safely assume $\Delta \geq 0$ without loss of generality.

The energy band at $B=0$ is given by

$$\varepsilon_s(p) = s\sqrt{v^2p^2 + \Delta^2} \quad (s = \pm 1), \tag{2}$$

with electron momentum $\mathbf{p}=(p_x,p_y)$ and $p=\sqrt{p_x^2+p_y^2}$. The density of states is[51]

$$D(\varepsilon) = \frac{g_v g_s |\varepsilon|}{2\pi\hbar^2 v^2}\theta(|\varepsilon| - |\Delta|), \tag{3}$$

where $g_s=2$ and $g_v=2$ represent the degrees of freedom associated with spin and valley, respectively, and $\theta(t)$ is a step function, defined by

$$\theta(t) = \begin{cases} 1 & (t>0) \\ 0 & (t<0). \end{cases} \tag{4}$$

The Landau-level spectrum can be found using the relation $\pi_+=(\sqrt{2}\hbar/l_B)a^\dagger$ and $\pi_-=(\sqrt{2}\hbar/l_B)a$, where $l_B=\sqrt{c\hbar/(eB)}$ is magnetic length and $a^\dagger$ and a are raising and lowering operators for usual Landau-level wave functions, respectively. The eigenenergy at K point becomes

$$\varepsilon_n^K = \mathrm{sgn}_-(n)\sqrt{(\hbar\omega_B)^2|n|+\Delta^2} \quad (n=0,\pm 1,\pm 2,\ldots), \tag{5}$$

where $\hbar\omega_B=\sqrt{2}\hbar v/l_B$ and

$$\mathrm{sgn}_\pm(n) = \begin{cases} +1 & (n>0) \\ \pm 1 & (n=0) \\ -1 & (n<0). \end{cases} \tag{6}$$

The corresponding wave function is

$$\Phi_n^K = \begin{pmatrix} \sin(\alpha_n/2)\phi_{|n|-1} \\ \cos(\alpha_n/2)\phi_{|n|} \end{pmatrix}, \tag{7}$$

where α_n satisfies

$$\sin\alpha_n = \frac{\hbar\omega_B\sqrt{|n|}\,\mathrm{sgn}_-(n)}{\sqrt{(\hbar\omega_B)^2|n|+\Delta^2}}, \tag{8}$$

$$\cos\alpha_n = -\frac{\Delta\,\mathrm{sgn}_-(n)}{\sqrt{(\hbar\omega_B)^2|n|+\Delta^2}}, \tag{9}$$

and ϕ_n is the usual Landau-level wave function, where ϕ_n with $n<0$ should be regarded as zero.

The Landau level $n=0$ lies just at the top of the valence band, i.e., $\varepsilon_0^K=-\Delta$ because $\alpha_0=0$, and its amplitude is only at the B site. Similarly, for Landau levels lying in the vicinity of the valence-band top, i.e., $n\leq 0$ satisfying $\hbar\omega_B\sqrt{|n|}\ll\Delta$, we have $\alpha_n\approx 0$, showing that the amplitude of the wave function is significant only at the B site. For those in the conduction band $n>0$, on the other hand, we have $\alpha_n\approx\pi$, showing that the amplitude is significant only at the A site.

For the K' point, on the other hand, the eigenenergy is given by Eq. (5) with $\mathrm{sgn}_-(n)$ being replaced with $\mathrm{sgn}_+(n)$ and the eigenfunction is given by

$$\Phi_n^{K'} = \begin{pmatrix} \sin(\alpha_n'/2)\phi_{|n|} \\ \cos(\alpha_n'/2)\phi_{|n|-1} \end{pmatrix}, \tag{10}$$

where α_n' is obtained from α_n by replacing $\mathrm{sgn}_-(n)$ with $\mathrm{sgn}_+(n)$. The Landau level $n=0$ lies just at the bottom of the conduction band, i.e., $\varepsilon_0^{K'}=+\Delta$ because $\alpha_0'=\pi$, and its amplitude is only at the A site. Similarly, for low-lying Landau levels in the conduction band $n\geq 0$, we have $\alpha_n'\approx\pi$, showing that the amplitude of the wave function is significant only at the A site. For those in the valence band $n<0$, on the other hand, we have $\alpha_n'\approx 0$, showing that the amplitude is significant only at the B site.

The Landau levels of $n\neq 0$ are doubly degenerate between the K and K' valleys, while those of $n=0$ are not. Therefore, by defining

$$\varepsilon_s(x_n) = s\sqrt{x_n+\Delta^2}, \tag{11}$$

$$x_n = (\hbar\omega_B)^2 n, \tag{12}$$

the thermodynamical potential at temperature T then becomes

$$\Omega = -\frac{1}{\beta}\frac{g_v g_s}{2\pi l_B^2}\sum_{s=\pm}\sum_{n=0}^{\infty}\varphi[\varepsilon_s(x_n)]\left(1-\frac{\delta_{n0}}{2}\right), \tag{13}$$

where $\beta=1/k_BT$ and

$$\varphi(\varepsilon) = \ln[1+e^{-\beta(\varepsilon-\zeta)}], \tag{14}$$

with ζ being the chemical potential.

In weak magnetic field, using the Euler-Maclaurin formula, the summation in n in Eq. (13) can be written as an integral in continuous variable x and a residual term as

$$\Omega = -\frac{1}{\beta}\frac{g_v g_s}{4\pi^2\hbar^2 v^2}\sum_{s=\pm}\left(\int_0^\infty \varphi[\varepsilon_s(x)]dx - \frac{(\hbar\omega_B)^4}{12}\frac{\partial\varphi[\varepsilon_s(x)]}{\partial x}\bigg|_{x=0}\right) + O[(\hbar\omega_B)^6]. \tag{15}$$

The expansion is valid when $\hbar\omega_B\ll k_BT$, or the Landau-level spacing is smaller than the thermal energy. The magnetization is given by

$$M = -\left(\frac{\partial\Omega}{\partial B}\right)_\zeta, \tag{16}$$

and the magnetic susceptibility by

$$\chi = \lim_{B\to 0}\frac{M}{B} = -\left(\frac{\partial^2\Omega}{\partial B^2}\right)_\zeta\bigg|_{B=0}. \tag{17}$$

In Eq. (15), the first term represents the thermodynamic potential in the absence of a magnetic field and only the second term depends on the magnetic field. We have

$$\chi = \int d\varepsilon\left(-\frac{\partial f}{\partial\varepsilon}\right)\chi(\varepsilon), \tag{18}$$

with

$$\chi(\varepsilon) = -g_v g_s\frac{e^2v^2}{6\pi c^2}\frac{1}{2|\Delta|}\theta(|\Delta|-|\varepsilon|), \tag{19}$$

where $f(\varepsilon)$ is the Fermi distribution function. The susceptibility at zero temperature is given by $\chi(\varepsilon_F)$ with ε_F being the Fermi energy. In the limit of $\Delta\to 0$, the susceptibility approaches a δ function,

$$\chi(\varepsilon) = -g_v g_s\frac{e^2v^2}{6\pi c^2}\delta(\varepsilon), \tag{20}$$

in agreement with the previous result.[1,21,23,40]

The susceptibility and the density of states, given by Eqs. (19) and (3), respectively, are shown in Fig. 1. Note that the upward direction represents negative (i.e., diamagnetic) susceptibility. The susceptibility is not zero at zero electron density, $-1<\varepsilon/|\Delta|<+1$, because the completely filled valence band gives a constant diamagnetic susceptibility. When the

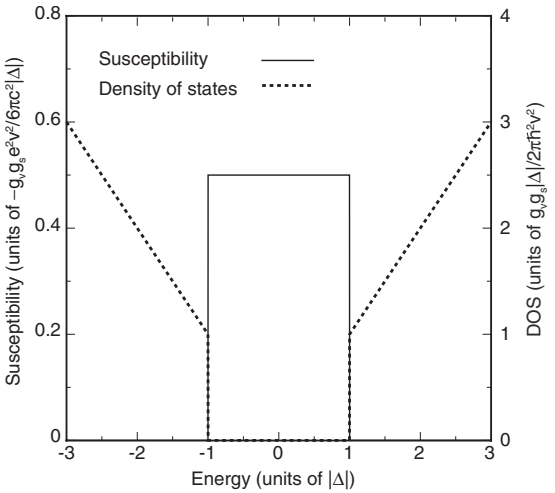

FIG. 1. Orbital susceptibility (solid line) and density of states (dashed line) of monolayer graphene with band gap Δ. Note that the upward direction represents negative (i.e., diamagnetic) susceptibility.

Fermi energy enters the conduction band, the susceptibility jumps downs to zero, resulting in zero total magnetism. In the limit of $\Delta \to 0$, the step height at the band edge increases in proportion to Δ^{-1} and the susceptibility approaches a δ function.

Because the Hamiltonian is equivalent to that of a Dirac electron with a nonzero mass, the magnetic susceptibility around the band edge should correspond to that of a conventional electron. This is clearly illustrated by the effective Hamiltonian expanded in the vicinity of $\mathbf{k}=0$. For the conduction band, $s=+1$, the effective Hamiltonian for the A site near the band bottom ($\varepsilon=\Delta$) is written apart from the constant energy as

$$\mathcal{H}^K \approx \frac{v^2}{2\Delta}\pi_-\pi_+ = \frac{\boldsymbol{\pi}^2}{2m^*} - \frac{1}{2}g^*\mu_B B, \tag{21}$$

$$\mathcal{H}^{K'} \approx \frac{v^2}{2\Delta}\pi_+\pi_- = \frac{\boldsymbol{\pi}^2}{2m^*} + \frac{1}{2}g^*\mu_B B, \tag{22}$$

where μ_B is the Bohr magneton, given by $e\hbar/(2mc)$ with m being the free-electron mass, and we used the relation $[\pi_x, \pi_y] = i\hbar eB/c$ and defined

$$m^* = \frac{\Delta}{v^2}, \quad g^* = 2\frac{m}{m^*}. \tag{23}$$

For instance, the g factor is estimated at $g^* \sim 60$ at $\Delta = 0.1$ eV, and diverges as $\propto \Delta^{-1}$ as the gap decreases. The last term in each Hamiltonian can be regarded as the pseudospin Zeeman term, where the different valleys K and K' serve as pseudospin up ($\xi=+1$) and down ($\xi=-1$), respectively. This agrees with the Zeeman energy expected for an intrinsic magnetic moment that originates from the self-rotation of the wave packet in Bloch electron.[54,55] The combined Hamiltonian is written as

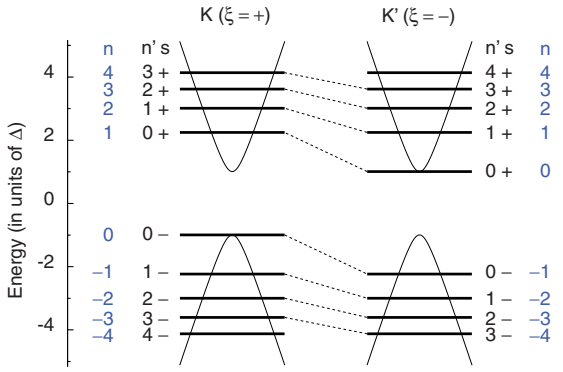

FIG. 2. (Color online) Landau-level energies of gapped monolayer graphene with $\hbar\omega_B = 2\Delta$. Dashed lines connecting the levels of K and K' represent corresponding levels with opposite pseudospins.

$$\mathcal{H} \approx \frac{\boldsymbol{\pi}^2}{2m^*} - \frac{\xi}{2}g^*\mu_B B. \tag{24}$$

Obviously, the pseudospin Zeeman term gives the Pauli paramagnetism and the first term containing $\boldsymbol{\pi}^2$ gives the Landau diamagnetism in the usual form as

$$\chi_P(\varepsilon) = \left(\frac{g^*}{2}\right)^2 \mu_B^2 D(\varepsilon), \tag{25}$$

$$\chi_L(\varepsilon) = -\frac{1}{3}\left(\frac{m}{m^*}\right)^2 \mu_B^2 D(\varepsilon), \tag{26}$$

with density of states

$$D(\varepsilon) = \frac{g_v g_s m^*}{2\pi\hbar^2}\theta(\varepsilon). \tag{27}$$

The total susceptibility $\chi_P + \chi_L$ actually agrees with the amount of the jump at the conduction band bottom in χ of Eq. (19). Because $g = 2m/m^*$ in the present case, we have $\chi_L = -\chi_P/3 \propto 1/m^*$ as in the free electron, giving the paramagnetic susceptibility in total. Therefore, the susceptibility exhibits a discrete jump toward the paramagnetic direction when the Fermi energy moves off the Dirac point. The jump height goes to infinity as the gap closes, because the susceptibility is inversely proportional to the effective mass. It should be noted that the quadratic approximation, Eq. (24), correctly gives a discrete jump at the band edge, while not the linear dependence on ε of the density of states off the edge, because the order of ε/Δ is neglected in this treatment.

In the original Hamiltonian, the Landau-level energies in Eq. (5) can be rewritten as

$$\varepsilon_{\xi,s,n'} = s\sqrt{(\hbar\omega_B)^2\left(n' + \frac{1}{2} + \frac{\xi s}{2}\right) + \Delta^2} \quad (n' = 0,1,2,\ldots). \tag{28}$$

Figure 2 shows energy levels for $\hbar\omega_B = 2\Delta$ and the relationship between the different labeling schemes of Eqs. (5) and (28). For the conduction band, the levels of the same n' with opposite pseudospins $\xi = \pm 1$ share the same Landau-level function $\phi_{n'}$ on the A site, on which the states near the

conduction-band bottom ($\varepsilon=\Delta$) have most of the amplitude as has been discussed above. For the valence band, similarly, n' describes the index of the Landau-level function at the B site.

III. BILAYER GRAPHENE

Bilayer graphene is a pair of graphene layers arranged in AB (Bernal) stacking and includes A_1 and B_1 atoms on layer 1 and A_2 and B_2 on layer 2.[29–37] The low-energy states are again given by the states around K and K' points in the Brillouin zone. The Hamiltonian at the K point for the basis $(|A_1\rangle,|B_1\rangle,|A_2\rangle,|B_2\rangle)$ is given by

$$\mathcal{H}^K=\begin{pmatrix} \Delta & v\pi_- & 0 & 0 \\ v\pi_+ & \Delta & \gamma_1 & 0 \\ 0 & \gamma_1 & -\Delta & v\pi_- \\ 0 & 0 & v\pi_+ & -\Delta \end{pmatrix}, \tag{29}$$

where $\gamma_1\approx 0.39$ eV (Ref. 56) represents interlayer coupling between B_1 and A_2,[29,30,57] and Δ describes potential asymmetry between layers 1 and 2 (not A and B sites), which gives rise to an energy gap.[29–33,35,57,58] The Hamiltonian at the K' point is obtained by exchanging $\pi_\pm$ in Eq. (29). Experimentally the potential asymmetry can be induced by applying an electric field perpendicular to the layer,[26–28,59,60] and the energy gap as large as 0.2 eV was actually observed in spectroscopic measurements.[26,59,60]

The energy band at $B=0$ is given by

$$\varepsilon_{s\mu}(p)=s\left(\frac{\gamma_1^2}{2}+v^2p^2+\Delta^2+\mu\left[\frac{\gamma_1^4}{4}+v^2p^2(\gamma_1^2+4\Delta^2)\right]^{1/2}\right)^{1/2}, \tag{30}$$

with $\mu=\pm 1$.[33] The indices $\mu=+1$ and -1 give a pair of bands further and closer to zero energy, respectively, and $s=+1$ and -1 in each pair represent the electron and hole branches, respectively. The band-edge energies corresponding to $p=0$ are given by $|\varepsilon|=\varepsilon_\pm$ for $\mu=\pm 1$, where

$$\varepsilon_+=\sqrt{\gamma_1^2+\Delta^2},\quad \varepsilon_-=|\Delta|. \tag{31}$$

For $\mu=-1$, the band minimum becomes

$$\varepsilon_0=\frac{\gamma_1|\Delta|}{\sqrt{\gamma_1^2+4\Delta^2}}, \tag{32}$$

which corresponds to an off-center momentum.[30] The density of states diverges here as $D(\varepsilon)\propto(\varepsilon-\varepsilon_0)^{-1/2}$. The energy bands and the density of states with several Δ's are plotted in Figs. 3(a) and 3(b), respectively. Vertical lines in Fig. 3(a) indicate the energies of ε_0, ε_-, and ε_+ for $\Delta=0.5\gamma_1$.

In a magnetic field, the eigenfunction of the Hamiltonian at the K point is written as $(c_1\phi_{n-1},c_2\phi_n,c_3\phi_n,c_4\phi_{n+1})$ with integer $n\geq -1$. For $n\geq 1$, the Hamiltonian matrix for (c_1,c_2,c_3,c_4) becomes[30,61]

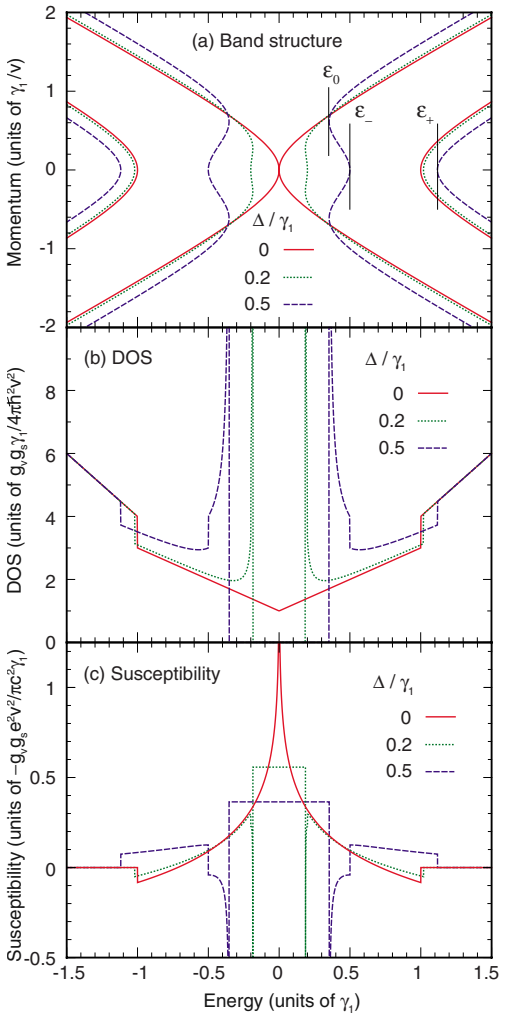

FIG. 3. (Color online) (a) Band structure, (b) density of states, and (c) susceptibility of bilayer graphenes with the asymmetry gaps $\Delta/\gamma_1=0$, 0.2, and 0.5. Vertical lines in (a) indicate the energies of ε_0, ε_-, and ε_+ for $\Delta/\gamma_1=0.5$. The upward direction represents negative (i.e., diamagnetic) susceptibility in (c).

$$H^K_{n\geq 1}=\begin{pmatrix} \Delta & \hbar\omega_B\sqrt{n} & 0 & 0 \\ \hbar\omega_B\sqrt{n} & \Delta & \gamma_1 & 0 \\ 0 & \gamma_1 & -\Delta & \hbar\omega_B\sqrt{n+1} \\ 0 & 0 & \hbar\omega_B\sqrt{n+1} & -\Delta \end{pmatrix}, \tag{33}$$

For $n=0$, the first component does not actually exist because $\phi_{-1}=0$. The matrix for (c_2,c_3,c_4) becomes

$$H^K_0=\begin{pmatrix} \Delta & \gamma_1 & 0 \\ \gamma_1 & -\Delta & \hbar\omega_B \\ 0 & \hbar\omega_B & -\Delta \end{pmatrix}. \tag{34}$$

For $n=-1$, only the component c_4 survives and the Hamiltonian is

$$H^K_{-1}=-\Delta. \tag{35}$$

For the K' point, the eigenfunction is written as $(c_1\phi_{n+1}, c_2\phi_n, c_3\phi_n, c_4\phi_{n-1})$. For $n \geq 1$, the Hamiltonian matrix for (c_1, c_2, c_3, c_4) is

$$H_{n\geq 1}^{K'} = \begin{pmatrix} \Delta & \hbar\omega_B\sqrt{n+1} & 0 & 0 \\ \hbar\omega_B\sqrt{n+1} & \Delta & \gamma_1 & 0 \\ 0 & \gamma_1 & -\Delta & \hbar\omega_B\sqrt{n} \\ 0 & 0 & \hbar\omega_B\sqrt{n} & -\Delta \end{pmatrix}. \tag{36}$$

For $n=0$, the matrix for (c_1, c_2, c_3) becomes

$$H_0^{K'} = \begin{pmatrix} \Delta & \hbar\omega_B & 0 \\ \hbar\omega_B & \Delta & \gamma_1 \\ 0 & \gamma_1 & -\Delta \end{pmatrix}, \tag{37}$$

and for $n=-1$ that for c_1 is

$$H_{-1}^{K'} = \Delta. \tag{38}$$

If we extend the definition of the matrix of Eq. (33) to $n=0$, its three eigenvalues agree with those of H_0^K and the rest with that of $H_{-1}^{K'}$. Similarly, the matrix of Eq. (36) with $n=0$ gives eigenvalues of $H_0^{K'}$ and H_{-1}^K. Thus, we can use Eqs. (33) and (36) with $n \geq 0$ to produce the full spectrum. By introducing the pseudospin variable $\xi = \pm 1$, the Hamiltonian is combined into a single expression,

$$H_n^\xi = \begin{pmatrix} \Delta & \sqrt{x_{n-}} & 0 & 0 \\ \sqrt{x_{n-}} & \Delta & \gamma_1 & 0 \\ 0 & \gamma_1 & -\Delta & \sqrt{x_{n+}} \\ 0 & 0 & \sqrt{x_{n+}} & -\Delta \end{pmatrix}, \tag{39}$$

with

$$x_{n\pm} = x_n \pm \frac{1}{2}\xi\delta, \tag{40}$$

$$x_n = \left(n + \frac{1}{2}\right)\delta, \quad \delta = (\hbar\omega_B)^2. \tag{41}$$

We write the eigenvalues of H_n^ξ as

$$\varepsilon_j(x_n, \xi\delta) \quad (j = 1,2,3,4), \tag{42}$$

in the ascending order in energy ($j=1$ and 2 for valence bands, and $j=3$ and 4 for the conduction bands). The second argument in $\varepsilon_j(x_n, \xi\delta)$ represents the dependence on B which is not included in x_n.

Figure 4 shows the example of the Landau-level spectrum at $\Delta/\gamma_1 = 0.2$ and $\hbar\omega_B/\gamma_1 = 0.5$, where the thick dashed lines represent the Landau level which originally belongs to $n=-1$ at opposite valleys. The correspondence between quantum numbers j and (s, μ) are indicated in the figure.

The thermodynamic potential becomes

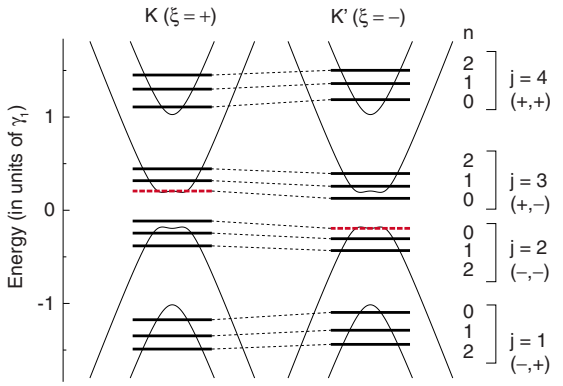

FIG. 4. (Color online) Landau-level energies of bilayer graphene given by Eq. (39) with $\Delta = 0.2\gamma_1$ and $\hbar\omega_B = 0.5\gamma_1$. At each valley, an energy level indicated as broken bar represents the Landau level, which originally belongs to $n=-1$ at opposite valley. The quantum number (s, μ) is indicated below j.

$$\begin{aligned} \Omega &= -\frac{1}{\beta}\frac{g_s}{2\pi l_B^2}\sum_{\xi,j}\sum_{n=0}^{\infty}\varphi[\varepsilon_j(x_n, \xi\delta)] \\ &= -\frac{1}{\beta}\frac{g_s}{4\pi\hbar^2 v^2}\sum_{\xi,j}\left[\int_0^\infty \varphi[\varepsilon_j(x, \xi\delta)]dx \right. \\ &\quad \left. + \frac{\delta^2}{24}\frac{\partial\varphi[\varepsilon_j(x,0)]}{\partial x}\bigg|_{x=0}\right] + O(\delta^3), \end{aligned} \tag{43}$$

where we used the Euler-Maclaurin formula in the second equation. The first term in the bracket can be transformed by changing the integral variable from x to ε as

$$\frac{1}{\beta}\int_0^\infty \varphi[\varepsilon_j(x, \xi\delta)]dx = \int_{-\infty}^\infty f(\varepsilon)n_j(\varepsilon, \xi\delta)d\varepsilon, \tag{44}$$

where we used $\varphi'(\varepsilon) = -\beta f(\varepsilon)$ and defined

$$n_j(\varepsilon, \xi\delta) \equiv s_j(\varepsilon, \xi\delta)x_j(\varepsilon, \xi\delta), \tag{45}$$

where $x_j(\varepsilon, \xi\delta)$ is a real and positive solution of $\varepsilon = \varepsilon_j(x, \xi\delta)$ and

$$s_j(\varepsilon, \xi\delta) \equiv \mathrm{sgn}\left(\frac{\partial x_j(\varepsilon, \xi\delta)}{\partial\varepsilon}\right). \tag{46}$$

If there are more than one solution of x_j, we regard n_j as their sum. The quantity $n_j(\varepsilon, \xi\delta)/(4\pi\hbar^2 v^2)$ represents the electron density below ε for the conduction band and the hole density above ε for the valence band.

By expanding

$$n_j(\varepsilon, \xi\delta) = n_j^{(0)}(\varepsilon) + n_j^{(1)}(\varepsilon)\xi\delta + \frac{1}{2}n_j^{(2)}(\varepsilon)\delta^2 + \cdots, \tag{47}$$

we can further expand Ω of Eq. (43) in terms of $\delta \propto B$. We have

$$\begin{aligned} \chi(\varepsilon) = g_s g_v \frac{e^2 v^2}{\pi c^2}\sum_j \left[\int_{-\infty}^{\varepsilon} n_j^{(2)}(\varepsilon')d\varepsilon' \right. \\ \left. - \frac{1}{12}\theta[\varepsilon - \varepsilon_j(0,0)]\frac{\partial\varepsilon_j(x,0)}{\partial x}\bigg|_{x=0}\right]. \end{aligned} \tag{48}$$

For the Hamiltonian of Eq. (39), the eigenequation $\det(\varepsilon - H_n^{\xi})=0$ can be solved for $x(\equiv x_n)$ as

$$x_{\pm} = \varepsilon^2 + \Delta^2 \pm \frac{1}{2}\sqrt{(4\varepsilon\Delta - \xi\delta)^2 + 4\gamma_1^2(\varepsilon^2 - \Delta^2)}, \quad (49)$$

which gives $x_j(\varepsilon, \xi\delta)$ when being real and positive. Let us first consider the case $\varepsilon > \varepsilon_+$, where two conduction bands are occupied by electrons. In this case $x_{\pm}$ are both real and positive and we have $x_1=x_2=0$, $x_3=x_+$, and $x_4=x_-$. Then, we have

$$\sum_j n_j(\varepsilon, \xi\delta) = x_+ + x_- = 2(\varepsilon^2 + \Delta^2), \quad (50)$$

independent of $\xi\delta$. Therefore, $\Sigma_j n_j^{(2)}(\varepsilon)$ identically vanishes, resulting in susceptibility independent of energy in the region $\varepsilon > \varepsilon_+$. The same is true for $\varepsilon < -\varepsilon_+$. Because $\chi=0$ for $\varepsilon = \pm\infty$, i.e., in the case of empty or filled band, we can conclude that the susceptibility vanishes for $\varepsilon > \varepsilon_+$ and $\varepsilon < -\varepsilon_+$ independent of interlayer interaction γ_1 and asymmetry Δ.

Similarly, the density of states for $|\varepsilon| > \varepsilon_+$ is independent of γ_1 and Δ and becomes twice as large as that of monolayer. In fact, we have

$$D(\varepsilon) \propto \frac{\partial}{\partial\varepsilon}\sum_j n_j(\varepsilon, 0) = 4\varepsilon. \quad (51)$$

This feature of the density of states is apparent in Fig. 3(b).

In the vicinity of the bottom of the excited conduction band, $\varepsilon=\varepsilon_+$, we have

$$n_4^{(2)}(\varepsilon) = \frac{\partial^2}{\partial\delta^2} x_-\theta(x_-)\bigg|_{\delta=0} = \left[\frac{\partial^2 x_-}{\partial\delta^2}\theta(x_-) + \left(\frac{\partial x_-}{\partial\delta}\right)^2 \delta(x_-)\right]_{\delta=0}, \quad (52)$$

where we used $x_-\delta(x_-)=0$ and $x_-\delta'(x_-)=-\delta(x_-)$. Using Eq. (48), we find that the susceptibility makes a discrete jump at ε_+ as

$$\chi(\varepsilon_+ + 0) - \chi(\varepsilon_+ - 0) = g_v g_s \frac{e^2 v^2}{\pi c^2}\left(\frac{\Delta^2\sqrt{\Delta^2 + \gamma_1^2}}{\gamma_1^2(2\Delta^2 + \gamma_1^2)} - \frac{2\Delta^2 + \gamma_1^2}{12\gamma_1^2\sqrt{\Delta^2 + \gamma_1^2}}\right), \quad (53)$$

where the first term in the brackets comes from the integral of the δ function in Eq. (52) and the second term from the step function in Eq. (48).

Near ε_+, the eigenstates are given primarily by the dimer states composed of $|B_1\rangle$ and $|A_2\rangle$. The effective Hamiltonian is described by the second order in interband interaction with the conduction-band bottom $|A_1\rangle$ and the valence-band top $|B_2\rangle$, where each process gives a term $\propto\pi_+\pi_-$ or $\propto\pi_-\pi_+$. In symmetric bilayer with $\Delta=0$, the terms $\pi_+\pi_-$ and $\pi_-\pi_+$ have the same coefficient and the pseudospin Zeeman term identically vanishes. When Δ becomes nonzero, the two coefficients shift from each other linearly in Δ because of the band-gap opening, leading to a nonzero Zeeman term. The resulting effective Hamiltonian is given by Eq. (24) with

$$m^* = \frac{\gamma_1^2\sqrt{\Delta^2 + \gamma_1^2}}{2v^2(2\Delta^2 + \gamma_1^2)}, \quad g^* = \frac{4\Delta\sqrt{\Delta^2 + \gamma_1^2}}{2\Delta^2 + \gamma_1^2}\frac{m}{m^*}. \quad (54)$$

In the region $\Delta \lesssim \gamma_1$, the typical magnitude of the effective mass m^* is on the order of $\sim\gamma_1/(2v^2)\approx 0.035m$.

The susceptibility is written as Pauli and Landau magnetism in Eqs. (25) and (26), respectively, which together give a susceptibility jump of Eq. (53). The paramagnetic component χ_P is zero at $\Delta=0$ and monotonically increases as Δ becomes larger. At $g^*=(2/\sqrt{3})(m/m^*)$ or $\Delta\approx 0.34\gamma_1$, χ_P exceeds χ_L and the susceptibility step changes from diamagnetic to paramagnetic. In the limit $\Delta\to\infty$, we have $g^*=2m/m^*$ as in the monolayer. This is to be expected, because the bilayer graphene in this limit can be regarded as a pair of independent monolayer graphenes, where interlayer coupling γ_1 opens an energy gap at each Dirac point. Similar argument also applies to the behavior around ε_-.

In the energy region $-\varepsilon_- < \varepsilon < -\varepsilon_0$ near the top of the valence band, both x_+ and x_- are real and positive, giving the states at outer and inner equienergy circles of the band $j=2$, respectively. Then we have

$$n_2^{(2)}(\varepsilon) = \frac{\partial^2}{\partial\delta^2}(-x_+ + x_-)\bigg|_{\delta=0} = \frac{\gamma_1^2(\Delta^2 - \varepsilon^2)}{2[(4\Delta^2 + \gamma_1^2)(\varepsilon^2 - \varepsilon_0^2)]^{3/2}}. \quad (55)$$

When the energy approaches $-\varepsilon_0$ from the negative side, the integral of $n_2^{(2)}(\varepsilon)$, thus the susceptibility, diverges in positive direction as $\propto(\varepsilon+\varepsilon_0)^{-1/2}$ in the same manner as the density of states. The same divergence occurs at the bottom of the conduction band, $+\varepsilon_0$, because of the electron-hole symmetry.

Full analytical expression of the susceptibility $\chi(\varepsilon)$ is complicated and presented in the Appendix. Figure 3(c) plots the susceptibility for $\Delta=0$, 0.2, and 0.5. In accordance with the above analytical consideration, we actually observe that the susceptibility vanishes in the regions $\varepsilon > \varepsilon_+$ and $\varepsilon < -\varepsilon_+$ and that the susceptibility step at $\varepsilon=\varepsilon_+$ changes from diamagnetic to paramagnetic with increasing Δ. We also see that the susceptibility for $\Delta\neq 0$ diverges in the paramagnetic direction at $\varepsilon=\pm\varepsilon_0$.

IV. THREE-DIMENSIONAL DIRAC SYSTEM

The results in monolayer graphene in Sec. II can be directly extended to three-dimensional Dirac Hamiltonian, which is also known to describe the approximate electronic structure of bismuth with strong spin-orbit interaction.[4–6,50] In bismuth, electronic states near the Fermi level is approximately described by a (4,4) matrix Hamiltonian, given by

$$\mathcal{H} = \begin{pmatrix} \Delta & 0 & v\pi_z & v\pi_- \\ 0 & \Delta & v\pi_+ & -v\pi_z \\ v\pi_z & v\pi_- & -\Delta & 0 \\ v\pi_+ & -v\pi_z & 0 & -\Delta \end{pmatrix}, \quad (56)$$

where four components consist of two orbital and two spin degrees of freedom, and the anisotropy of the velocity is ignored for simplicity. The orbital susceptibility was previ-

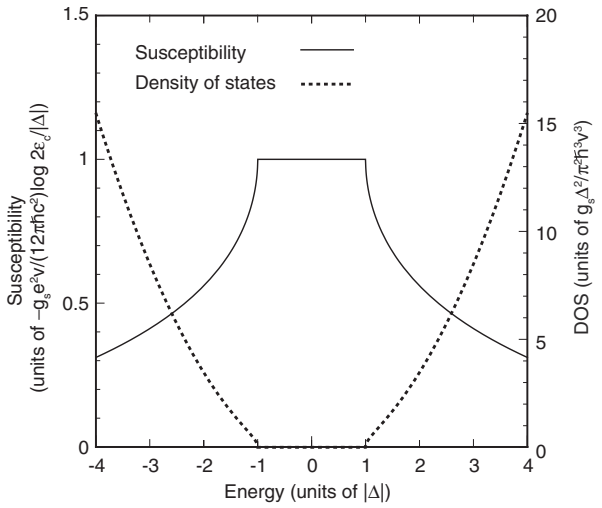

FIG. 5. Orbital susceptibility and density of states of three-dimensional Dirac electron.

ously calculated for realistic Hamiltonian retaining the anisotropy and other factors,[6] while here we work on the simplest Hamiltonian, Eq. (56), to focus on the parallel argument to its two-dimensional counterpart.

The density of states at zero magnetic field is

$$D(\varepsilon) = \frac{g_v g_s}{\pi^2\hbar^3 v^3}|\varepsilon|\sqrt{\varepsilon^2-\Delta^2}\,\theta(\varepsilon^2-\Delta^2), \tag{57}$$

where g_v is the valley degeneracy allowing the presence of different k points described by the above Hamiltonian in the first Brillouin zone. The Landau levels in a uniform magnetic field in z direction are given by

$$\varepsilon_{s,n,\sigma} = s\sqrt{(\hbar\omega_B)^2\left(n+\frac{1}{2}+\frac{\sigma}{2}\right)+v^2p_z^2+\Delta^2} \quad (n=0,1,2,\ldots), \tag{58}$$

with $\hbar\omega_B=\sqrt{2}\hbar v/l_B$, $s=\pm 1$, and $\sigma=\pm 1$. This is equivalent to the two-dimensional Dirac system, Eq. (28), when the term Δ^2 is replaced with $\Delta^2+v^2p_z^2$. The susceptibility $\chi(\varepsilon)$ is calculated by integrating Eq. (19) in p_z as

$$\chi(\varepsilon) = -\frac{g_v g_s e^2 v^2}{6\pi c^2}\int\frac{dp_z}{2\pi\hbar}\frac{\theta(\Delta^2+v^2p_z^2-\varepsilon^2)}{2\sqrt{\Delta^2+v^2p_z^2}}$$
$$= -\frac{g_v g_s e^2 v}{12\pi^2\hbar c^2}\begin{cases}\ln\dfrac{2\varepsilon_c}{|\Delta|} & (|\varepsilon|<|\Delta|)\\ \ln\dfrac{2\varepsilon_c}{|\varepsilon|+\sqrt{\varepsilon^2-\Delta^2}} & (|\varepsilon|>|\Delta|),\end{cases} \tag{59}$$

where ε_c is a cutoff energy. In the limit of $\Delta\to 0$, the susceptibility at zero energy logarithmically diverges.

At an energy ε just above the band bottom $|\Delta|$, we obtain the paramagnetic contribution

$$\chi(\varepsilon)-\chi(0) \approx \frac{2}{3}\left(\frac{m}{m^*}\right)^2 D(\varepsilon)\mu_B^2, \tag{60}$$

where $D(\varepsilon)=(g_s g_v/4\pi^2)(2m^*/\hbar^2)^{3/2}\sqrt{\varepsilon}$ with $m^*=\Delta/v^2$. This is nothing but the magnetic susceptibility, dominated by the Pauli paramagnetism, of a three-dimensional metal with mass m^* and a g factor $g^*=2m/m^*$. Figure 5 shows the susceptibility and the density of states in the present system. The singular decrease in the susceptibility at the band edges is fully understood in terms of the appearance of the dominant spin paramagnetism inside the band.

We note that in bismuth the index σ in Eq. (58) represents real spin, while it was valley pseudospin in Eq. (28) for graphene. The Pauli component included in Eq. (60) thus describes the real spin paramagnetism enhanced by the strong spin-orbit coupling, apart from the bare electron paramagnetism. As another remark, the chemical potential in intrinsic bismuth lies in the conduction band near the band bottom, while it can be controlled by changing the external pressure or the alloy concentration.[50]

V. CONCLUSION

We have calculated the orbital magnetism of narrow gap electronic systems described by the Dirac Hamiltonian, and found that singular behavior of the susceptibility near the band gap can be understood in terms of pseudospin Pauli paramagnetism induced by extra orbital degree of freedom. This has been demonstrated by explicit calculations of orbital susceptibility in monolayer and bilayer graphenes in the presence of band gap, as well as three-dimensional Dirac systems such as bismuth. In an analogous way to conventional metal, the susceptibility near the band edge can be expressed by the Landau diamagnetism and the Pauli paramagnetism associated with pseudospin. The diverging magnetism in intrinsic zero-gap graphene, which is previously known, can be intuitively interpreted as a result of vanishing the effective mass.

The susceptibility in the vicinity of the energy gap is typically on the order of $(m/m^*)^2\mu_B^2 D(\varepsilon)$ and overwhelms the real-spin Pauli paramagnetism of bare electrons, owing to small effective mass m^*. Particularly, we expect that the singular susceptibility in graphenes is observed by employing the experimental techniques used for two-dimensional electron systems on semiconductor.[62,63]

ACKNOWLEDGMENTS

This work was supported in part by Grant-in-Aid for Scientific Research on Priority Area "Carbon Nanotube Nanoelectronics," by Grant-in-Aid for Scientific Research, and by Global Center of Excellence Program at Tokyo Tech "Nanoscience and Quantum Physics" from the Ministry of Education, Culture, Sports, Science and Technology, Japan.

APPENDIX: SUSCEPTIBILITY OF BILAYER GRAPHENE

Using Eqs. (48) and (49), the susceptibility of $\chi(\varepsilon)$ of bilayer graphene with energy gap is calculated as

$$\chi(\varepsilon) = g_v g_s \frac{e^2 v^2}{\pi c^2 \gamma_1} \tilde{\chi}(\varepsilon), \tag{A1}$$

with

$$\tilde{\chi}(\varepsilon) = \begin{cases} \tilde{\chi}_0 + \tilde{\chi}_- + \tilde{\chi}_+ & (|\varepsilon| < \varepsilon_0) \\ 2F(\varepsilon) + \tilde{\chi}_- + \tilde{\chi}_+ & (\varepsilon_0 < |\varepsilon| < \varepsilon_-) \\ F(\varepsilon) + \tilde{\chi}_+ & (\varepsilon_- < |\varepsilon| < \varepsilon_+) \\ 0 & (\varepsilon_+ < |\varepsilon|), \end{cases} \tag{A2}$$

where

$$F(\varepsilon) = \frac{\gamma_1 \Delta^2 |\varepsilon|}{(\gamma_1^2 + 4\Delta^2)\sqrt{\gamma_1^2(\varepsilon^2 - \Delta^2) + 4\Delta^2\varepsilon^2}} + \frac{\gamma_1^3}{4(\gamma_1^2 + 4\Delta^2)^{3/2}} \ln[2|\varepsilon|(\gamma_1^2 + 4\Delta^2) + 2\sqrt{\gamma_1^2 + 4\Delta^2}\sqrt{\gamma_1^2(\varepsilon^2 - \Delta^2) + 4\Delta^2\varepsilon^2}], \tag{A3}$$

$$\tilde{\chi}_0 = \frac{\gamma_1^3 \ln[4\gamma_1^2\Delta^2(\gamma_1^2 + 4\Delta^2)]}{4(\gamma_1^2 + 4\Delta^2)^{3/2}}, \tag{A4}$$

$$\tilde{\chi}_- = -F(\varepsilon_-) + \frac{|\Delta|}{3\gamma_1}, \tag{A5}$$

$$\tilde{\chi}_+ = -F(\varepsilon_+) - \frac{\Delta^2\sqrt{\Delta^2 + \gamma_1^2}}{\gamma_1(2\Delta^2 + \gamma_1^2)} + \frac{2\Delta^2 + \gamma_1^2}{12\gamma_1\sqrt{\Delta^2 + \gamma_1^2}}. \tag{A6}$$

In the symmetric bilayer with vanishing gap, $\Delta = 0$, in particular, we simply get

$$\chi(\varepsilon) = g_v g_s \frac{e^2 v^2}{\pi c^2 \gamma_1} \theta(\gamma_1 - |\varepsilon|)\left(\frac{1}{4}\ln\frac{|\varepsilon|}{\gamma_1} + \frac{1}{12}\right), \tag{A7}$$

which agrees with the previous results.[38,39]

[1] J. W. McClure, Phys. Rev. **104**, 666 (1956).
[2] J. W. McClure, Phys. Rev. **119**, 606 (1960).
[3] M. P. Sharma, L. G. Johnson, and J. W. McClure, Phys. Rev. B **9**, 2467 (1974).
[4] P. A. Wolff, J. Phys. Chem. Solids **25**, 1057 (1964).
[5] H. Fukuyama and R. Kubo, J. Phys. Soc. Jpn. **27**, 604 (1969).
[6] H. Fukuyama and R. Kubo, J. Phys. Soc. Jpn. **28**, 570 (1970).
[7] K. S. Novoselov, A. K. Geim, S. V. Morozov, D. Jiang, Y. Zhang, S. V. Dubonos, I. V. Grigorieva, and A. A. Firsov, Science **306**, 666 (2004).
[8] K. S. Novoselov, A. K. Geim, S. V. Morozov, D. Jiang, M. I. Katsnelson, I. V. Grigorieva, S. V. Dubonos, and A. A. Firsov, Nature (London) **438**, 197 (2005).
[9] Y. Zhang, Y.-W. Tan, H. L. Stormer, and P. Kim, Nature (London) **438**, 201 (2005).
[10] J. C. Slonczewski and P. R. Weiss, Phys. Rev. **109**, 272 (1958).
[11] D. P. DiVincenzo and E. J. Mele, Phys. Rev. B **29**, 1685 (1984).
[12] G. W. Semenoff, Phys. Rev. Lett. **53**, 2449 (1984).
[13] N. H. Shon and T. Ando, J. Phys. Soc. Jpn. **67**, 2421 (1998).
[14] Y. Zheng and T. Ando, Phys. Rev. B **65**, 245420 (2002).
[15] T. Ando, J. Phys. Soc. Jpn. **74**, 777 (2005).
[16] V. P. Gusynin and S. G. Sharapov, Phys. Rev. Lett. **95**, 146801 (2005).
[17] N. M. R. Peres, F. Guinea, and A. H. Castro Neto, Phys. Rev. B **73**, 125411 (2006).
[18] S. G. Sharapov, V. P. Gusynin, and H. Beck, Phys. Rev. B **69**, 075104 (2004).
[19] H. Fukuyama, J. Phys. Soc. Jpn. **76**, 043711 (2007).
[20] M. Nakamura, Phys. Rev. B **76**, 113301 (2007).
[21] M. Koshino and T. Ando, Phys. Rev. B **75**, 235333 (2007).
[22] A. Ghosal, P. Goswami, and S. Chakravarty, Phys. Rev. B **75**, 115123 (2007).
[23] T. Ando, Physica E **40**, 213 (2007).
[24] M. Koshino, Y. Arimura, and T. Ando, Phys. Rev. Lett. **102**, 177203 (2009).
[25] K. S. Novoselov, E. McCann, S. V. Morozov, V. I. Falko, M. I. Katsnelson, U. Zeitler, D. Jiang, F. Schedin, and A. K. Geim, Nat. Phys. **2**, 177 (2006).
[26] T. Ohta, A. Bostwick, T. Seyller, K. Horn, and E. Rotenberg, Science **313**, 951 (2006).
[27] E. V. Castro, K. S. Novoselov, S. V. Morozov, N. M. R. Peres, J. M. B. Lopes dos Santos, J. Nilsson, F. Guinea, A. K. Geim, and A. H. Castro Neto, Phys. Rev. Lett. **99**, 216802 (2007).
[28] J. B. Oostinga, H. B. Heersche, X.-L. Liu, A. F. Morpurgo, and L. M. K. Vandersypen, Nat. Mater. **7**, 151 (2008).
[29] E. McCann and V. I. Falko, Phys. Rev. Lett. **96**, 086805 (2006).
[30] F. Guinea, A. H. Castro Neto, and N. M. R. Peres, Phys. Rev. B **73**, 245426 (2006).
[31] C. L. Lu, C. P. Chang, Y. C. Huang, J. M. Lu, C. C. Hwang, and M. F. Lin, J. Phys.: Condens. Matter **18**, 5849 (2006).
[32] C. L. Lu, C. P. Chang, Y. C. Huang, R. B. Chen, and M. L. Lin, Phys. Rev. B **73**, 144427 (2006).
[33] E. McCann, Phys. Rev. B **74**, 161403(R) (2006).
[34] M. Koshino and T. Ando, Phys. Rev. B **73**, 245403 (2006).
[35] J. Nilsson, A. H. Castro Neto, N. M. R. Peres, and F. Guinea, Phys. Rev. B **73**, 214418 (2006).
[36] B. Partoens and F. M. Peeters, Phys. Rev. B **74**, 075404 (2006).
[37] B. Partoens and F. M. Peeters, Phys. Rev. B **75**, 193402 (2007).
[38] S. A. Safran, Phys. Rev. B **30**, 421 (1984).
[39] M. Koshino and T. Ando, Phys. Rev. B **76**, 085425 (2007).
[40] S. A. Safran and F. J. DiSalvo, Phys. Rev. B **20**, 4889 (1979).
[41] J. Blinowski and C. Rigaux, J. Phys. (Paris) **45**, 545 (1984).
[42] R. Saito and H. Kamimura, Phys. Rev. B **33**, 7218 (1986).
[43] H. Ajiki and T. Ando, J. Phys. Soc. Jpn. **62**, 1255 (1993).
[44] H. Ajiki and T. Ando, J. Phys. Soc. Jpn. **62**, 2470 (1993); **63**, 4267 (1994) (Erratum).
[45] H. Ajiki and T. Ando, J. Phys. Soc. Jpn. **64**, 4382 (1995).
[46] M. Yamamoto, M. Koshino, and T. Ando, J. Phys. Soc. Jpn. **77**, 084705 (2008).
[47] M. Nakamura and L. Hirasawa, Phys. Rev. B **77**, 045429 (2008).
[48] A. H. Castro Neto, F. Guinea, N. M. Peres, K. S. Novoselov, and A. K. Geim, Rev. Mod. Phys. **81**, 109 (2009).

[49] A. Kobayashi, Y. Suzumura, and H. Fukuyama, J. Phys. Soc. Jpn. **77**, 064718 (2008).
[50] Y. Fuseya, M. Ogata, and H. Fukuyama, Phys. Rev. Lett. **102**, 066601 (2009).
[51] A. W. W. Ludwig, M. P. A. Fisher, R. Shankar, and G. Grinstein, Phys. Rev. B **50**, 7526 (1994).
[52] S. Y. Zhou, G.-H. Gweon, A. V. Fedorov, P. N. First, W. A. de Heer, D.-H. Lee, F. Guinea, A. H. Castro Neto, and A. Lanzara, Nat. Mater. **6**, 770 (2007).
[53] S. Y. Zhou, D. A. Siegel, A. V. Fedorov, F. El Gabaly, A. K. Schmid, A. H. Castro Neto, D.-H. Lee, and A. Lanzara, Nat. Mater. **7**, 259 (2008).
[54] M.-C. Chang and Q. Niu, Phys. Rev. B **53**, 7010 (1996).
[55] D. Xiao, W. Yao, and Q. Niu, Phys. Rev. Lett. **99**, 236809 (2007).
[56] A. Misu, E. Mendez, and M. S. Dresselhaus, J. Phys. Soc. Jpn. **47**, 199 (1979).
[57] T. Ando and M. Koshino, J. Phys. Soc. Jpn. **78**, 034709 (2009).
[58] T. Ando and M. Koshino, J. Phys. Soc. Jpn. **78**, 104716 (2009).
[59] Y. Zhang, T.-T. Tang, C. Girit, Z. Hao, M. C. Martin, A. Zettl, M. F. Crommie, Y. R. Shen, and F. Wang, Nature (London) **459**, 820 (2009).
[60] K. F. Mak, C. H. Lui, J. Shan, and T. F. Heinz, Phys. Rev. Lett. **102**, 256405 (2009).
[61] M. Koshino and E. McCann, Phys. Rev. B **81**, 115315 (2010).
[62] H. L. Stormer, T. Haavasoja, V. Narayanamurti, A. C. Gossard, and W. Wiegmann, J. Vac. Sci. Technol. B **1**, 423 (1983).
[63] J. P. Eisenstein, H. L. Stormer, V. Narayanamurti, A. Y. Cho, A. C. Gossard, and C. W. Tu, Phys. Rev. Lett. **55**, 875 (1985).